Journal of Applied Polymer Science

Fabrication of hierarchically crystallographic morphologies in isotactic polypropylene

Ming Wang, Jia Yuan, Shi-Hui Luo, Jian-Bing Zeng
School of Chemistry and Chemical Engineering, Southwest University, ChongQing 400715, China
Correspondence to: M. Wang (E-mail: mwang@swu.edu.cn) and J.-B. Zeng (E-mail: jbzeng@swu.edu.cn)

ABSTRACT: The hierarchically crystallographic morphologies were fabricated in isotactic polypropylene (iPP) by controlling the stratified distribution of the nucleating agents. The α- and β-nucleating agents were chosen for preparing the different crystalline modifications. The transcrystals and spherulites were found in the stratified distribution samples by polar optical microscopy (POM) and scanning electron microscope (SEM). The transcrystals grew from the surfaces of the nucleating agents filled layers and occupied most space of the pure iPP layers. The crystalline modifications and crystallinity were analyzed by X-ray diffraction (XRD) and differential scanning calorimeter (DSC) analysis. The mechanical and thermal degradation properties of these samples with hierarchically crystallographic morphologies were investigated by tensile testing machine and thermogravimetric analysis (TGA) respectively, and showed better than that of the samples with single crystallographic morphology (spherulites). © 2015 Wiley Periodicals, Inc. J. Appl. Polym. Sci. **2015**, *132*, 42703.

KEYWORDS: crystallization; mechanical properties; morphology

Received 30 March 2015; accepted 29 June 2015
DOI: 10.1002/app.42703

INTRODUCTION

Isotactic polypropylene (iPP) has many desirable and beneficial properties, such as a high melting point, a high tensile modulus, good toughness, excellent chemical resistance, and easy recycling, which make it useful for many industrial applications. However, the ultimate physical/chemical properties of iPP are directly related to its internal hierarchical structures, which range from the molecular, nanometer, submicron, and micron scale to the mesoscopic level. The wide range of applications of iPP results from its hierarchical structures, especially polymorphic crystals including monoclinic α-crystal, trigonal β-crystal, orthorhombic γ-crystal, and smectic mesophase.[1–6] The monoclinic α-crystal is a thermodynamically stable phase and predominates under normal processing conditions. They usually show excellent modulus, tensile strength but inferior ductility.[7–9] The trigonal β-crystals are a thermodynamically metastable phase. They exhibit excellent impact strength, especially at low temperatures.[10–15] The orthorhombic γ-crystal and smectic mesophase are less frequently observed in iPP.[16–18]

In most cases, polymer crystallization controls the polymer's structural formation and, thereby, strongly influences the final product's properties particularly mechanical, barrier, and optical properties. How to fabricate the precisely hierarchical crystal structures of iPP and finally control its properties has been attracted much attention. By using appropriate processing parameters, e.g., temperature and stress fields, the crystalline polymorphism can be prominently impacted, leading to significant variations in the ultimate hierarchical structure.[19–31] Some successfully processing methods have been reported to control the hierarchical structure of iPP articles, such as the in-process morphology control of injection molding,[26,27] multilayer coextrusion,[28,29] and *in situ* microfibrillation.[30,31]

Besides the processing strategies, adding nucleating agents with the ability of self-organizing in polymer melt is believed to be another important method to manipulate crystal morphology as well as properties of polymer articles. Take the formation of β-crystals in iPP for example, the method of adding β-nucleating agents can induce high concentration of β-crystals and has some additional advantages, such as addition of very low nucleator content, little influence on the processing properties of iPP, and high performance/cost ratio comparing with processing approaches.[32–35] Using the combined effects of shear flow and β-nucleating agents, the iPP samples with both high strength and nice toughness can be fabricated by an industrial injection molding machine.[36]

Transcrystals are well-known structural features in polymers, which occur as the result of overgrowth of the polymer crystals on the surface of the molded articles, especially the organic and inorganic fibers.[37] The heterogeneous nucleation occurs with a high density of active nuclei at the article surface, and then the

crystal growth is restricted to the lateral direction so that a columnar layer develops around the article.[38–42] This type of directional crystal growth can yield substantial molecular orientation within the transcrystalline layers and thus influence the properties of the material. In our previous study, the transcrystallization could be tuned by controlling the distribution of fillers, i.e., the stratified distribution, and then enhanced the mechanical properties of the composites.[43,44]

In this work, the development of hierarchically crystallographic morphologies including α-crystals (α-spherulites and α-transcrystals) and β-crystals (β-spherulites and β-transcrystals) in iPP was manipulated by controlling the stratified distribution of α- or β-nucleating agents (α- or β-NAs). The crystallization behavior and polymorphism of iPP including transcrystals have been intensively investigated together with its mechanical and thermal stabilization properties, which enables us to better tailor its properties.

EXPERIMENTAL

Materials

A commercially available Ziegler-Natta iPP was manufactured by Lanzhou Petroleum Chemical Incorporation (Gansu, China), with a melt flow index of 2.5 g/10 min (190°C, 2.16 kg), M_w = 399,000, M_w/M_n = 4.6, and a density of 0.90 g/cm^3−0.91 g/cm^3. The α-NAs (1, 3: 2, 4-dibenzylidene sorbitol, a typical sorbitol based clarifier) with trade names of TM-3 were pursued from Fine Chemical Institute, Shanxi, China. The β-NAs which were aryl amide compounds (TMB-5) were also supplied by Fine Chemical Institute, Shanxi, China.

Sample Preparation

Preparation of Nucleated iPP. The iPP and 0.25 wt % nucleating agents (NAs) (α-NAs or β-NAs) were first melt mixed with in a batch mixer. The temperature of mastication was about 180°C, the rotor rate was 30 rpm, and the mixing time was set at 5 min. The pure iPP without nucleating agents were also prepared under the same processing conditions for comparison. After the melt-mixing, the pure iPP, iPP with 0.25 wt % α- and β-NAs were then molded in a rectangle shape (10 cm × 10 cm) with ca. 1.0 mm thickness by a compression molding with a press of 10 MPa at 200°C for 15 min, respectively. The sheets were finally cooled down to room temperature with a press of 10 MPa at ca 40°C/min. The dog-bone samples were cut directly from the sheets for the tensile test. For convenience, iPP with 0.25 wt % α- and β-NAs were designated as iPP/α-NA and iPP/β-NA, respectively.

Preparation of Nucleated iPP with Stratified Distribution. First, four thin films of the nucleated iPP with 0.5 wt % α- and β-NAs with ca. 0.12 mm thickness were prepared by conventional compression molding with a press of 10 MPa at 200°C for 5 min, respectively. The thin sheets were finally cooled down to room temperature with a press of 10 MPa at ca 40°C/min. Five thin films of pure iPP with 0.12 mm thickness were also molded at the same condition. Second, the above nine films were alternately sandwiched with iPP films at surface, and then compressed with a press of 10 MPa at 200°C for 10 min and finally cooled down to room temperature with a press of 10 MPa at ca 40°C/min to form the final composites (10 cm × 10 cm) with ca.1.0 mm in thickness. Three kinds of iPP with stratified distribution of nucleating agents are fabricated for the investigation and are named as M-iPP/α-NA, M-iPP/β-NA, M-iPP/α-NA/β-NA, respectively, as illustrated in Figure 1. Before sandwiching, all the thin films were washed by alcohol to make sure no dust on the surfaces. Finally, the iPP with stratified distribution of nucleating agents were successfully prepared by this two-step molding. The dog-bone samples were cut directly from these sandwiched sheets for the tensile test.

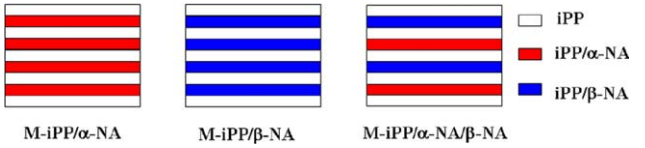

Figure 1. Schematic draws of the iPP with stratified distribution of α- or β-nucleating agents. [Color figure can be viewed in the online issue, which is available at wileyonlinelibrary.com.]

Measurement

Polar Optical Microscopy. The transcrystalline morphologies of the samples were investigated by a polar optical microscopy (POM, Olympus, BX51-P). A slice with 15 μm thickness was cryogenically microtomed from the samples at the thickness direction for the observation.

Differential Scanning Calorimetry. The thermal crystallization characteristics of the samples were studied by a differential scanning calorimeter (DSC) (TA DSC 204) using nitrogen as a purge gas. The nonisothermal crystalline behavior of the specimens was obtained through melting the samples (about 5 mg) from 25°C at a heating rate of 10°C/min to 220°C, and then maintained this temperature for 5 min to remove any thermal history and then cooling them to 25°C at 10°C/min, and finally heating them to 220°C at a heating rate of 10°C/min.

X-ray Diffraction. Wide angle X-ray diffraction (WAXD) analysis was performed on a MSAL-XD 3 (Beijing Purkinje General Instrument, China), using a Cu Kα radiation with a wavelength of 1.54 Å (36 kV and 20 mA). Scanning was performed over the angle range 2θ = 10–40° with a scanning rate of 4°/min. The relative content of β-crystal, K_β, was calculated according to the equations suggested by Turner-Jones *et al.*[2] and modified by Hsiao *et al.*[12,45]

Scanning Electron Microscope. The hierarchically crystallographic morphologies and the fracture behavior of the samples were characterized by an S3000N Hitachi scanning electron-microscope (SEM). For the observation of the hierarchically crystallographic morphologies, the samples were firstly cryogenically fractured in liquid nitrogen and then etched by 1% solution of potassium permanganate in a 10 : 4 : 1 (by volume) mixture, of concentrated sulphuric acid, 85% orthophosphoric acid and water, to remove the amorphous part of iPP.[43] To investigate the fracture behavior of the samples, the tensile fracture surfaces of the samples were directly coated with gold and then examined by the SEM.

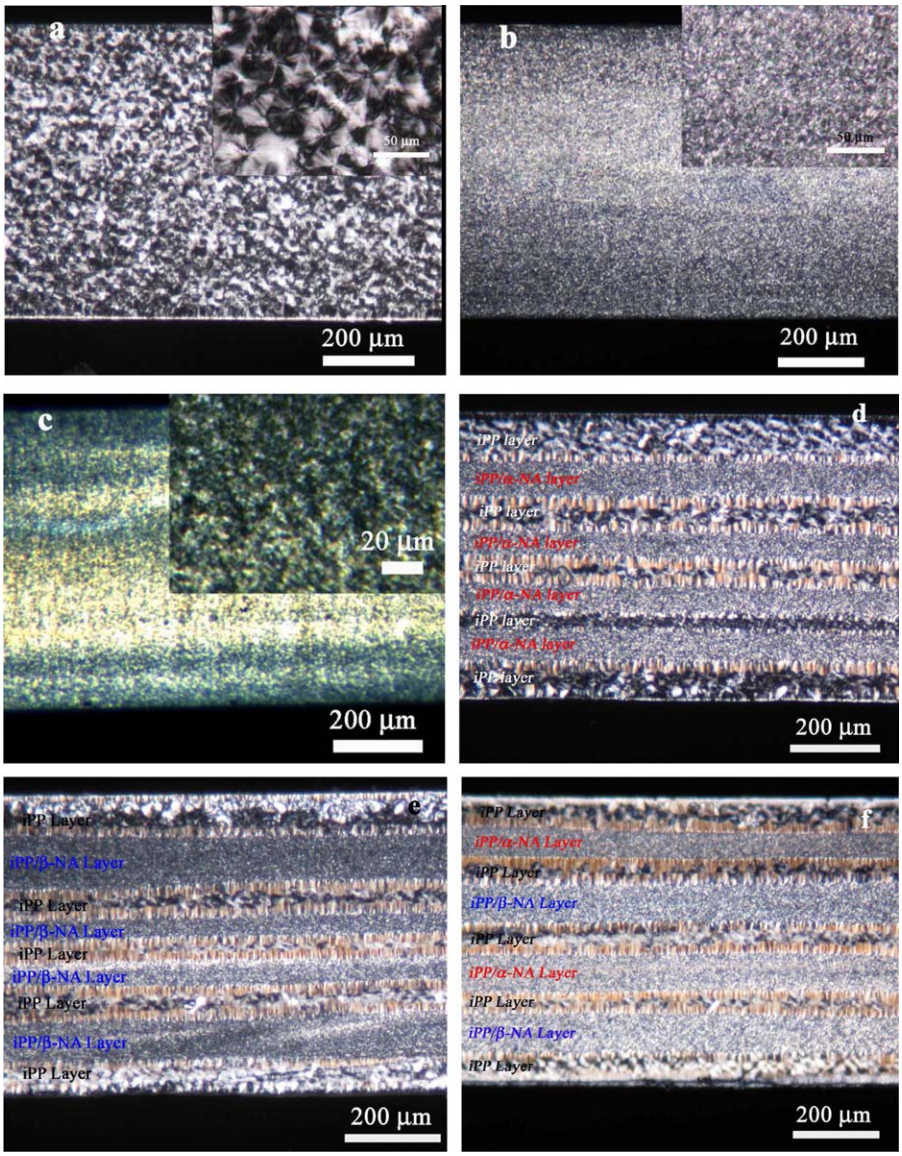

Figure 2. POM images of pure iPP (a), iPP/α-NA (b), iPP/β-NA (c), M-iPP/α-NA (d), M-iPP/β-NA (e), and M-iPP/α-NA/β-NA (f). [Color figure can be viewed in the online issue, which is available at wileyonlinelibrary.com.]

Tensile Experiment. Tensile tests were performed on dog-bone samples at 20 mm/min using an Instron universal tensile testing machine according to ASTM D-638. The measured temperature was set at 23 ± 2°C. The average values from at least five samples were reported.

Thermogravimetric Analysis. The thermogravimetric analysis (TGA) was also performed to study the thermal stability of iPP with hierarchically crystallographic morphologies at a heating rate of 10°C/min from room temperature to 600°C under nitrogen flow (50 mL/min), by a TA Q600 analyzer.

RESULTS AND DISCUSSION

Hierarchically Crystallographic Morphologies

Figure 2 shows the POM photographs of the nucleated iPP with stratified distribution samples together with the correspondingly conventional samples. The addition of nucleating agents reduced the spherulite size of pure iPP, but all the conventional samples exhibited homogeneous crystalline morphologies [Figure 2(a–c)]. In order to fabricate the hierarchically crystallographic morphologies, the nucleating agents were confined distribution in the strips. There were three kinds of crystallographic morphologies in the photographs, the small spherulites in layers with the nucleating agents, the transcrystals at the interfaces and large spherulites in the pure iPP layers. The transcrystals grew from the layers filled with nucleating agents into the pure iPP layers. Normally, the α-crystals are preferred formed in iPP at conventional processing conditions. However, the β-crystals can be obtained by adding β-nucleating agents which suppress the formation of the α-crystals.[13] Thus, the α-NAs in the iPP/α-NA layers probably formed α-transcrystals in the adjacent iPP layers while β-NAs formed β-transcrystals.

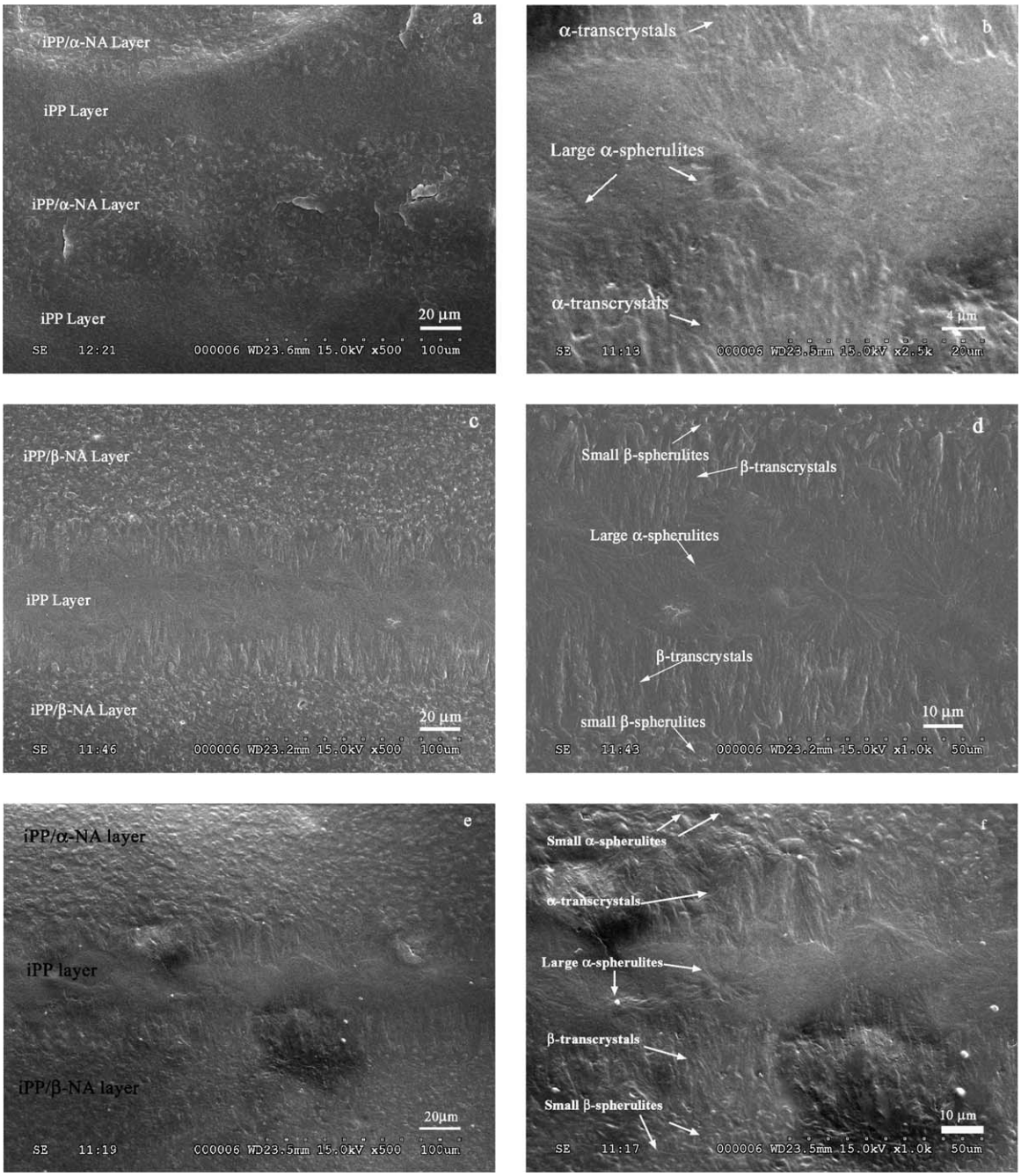

Figure 3. SEM images of the iPP with stratified distribution of α-NAs (a, b), *β*-NAs (c, d), and both α-NAs and *β*-NAs (e, f).

Figure 3 shows the SEM images of the iPP with stratified distribution of α- NAs, *β*-NAs, or both α-NAs and *β*-NAs. In the M-iPP/α-NA samples, the crystals of iPP included small α-spherulites, large α-spherulites and α-transcrystals. The small *β*-spherulites, large α-spherulites and *β*-transcrystals could be found in the M-iPP/*β*-NA samples, as shown in Figure 3(d). However, in the M-iPP/α-NA/*β*-NA samples, the hierarchically crystallographic morphologies consisted of small α-spherulites, small *β*-spherulites, large α-spherulites, α-transcrystals, and *β*-transcrystals [Figure 3(f)].

In Figure 3, we also found that the size of α-spherulites formed in the layers with α-NAs was larger than that of *β*-spherulites in the layers with *β*-NAs at the same content of NAs. Furthermore, the thickness of the *β*-transcrystals was thicker than that of the α-transcrystals because of the higher nucleation ability of iPP with *β*-NAs.

Crystallization Behavior

The nucleation ability of iPP with NAs can be evaluated by the nonisothermal crystallization study. Figure 4(a) gives the DSC cooling curves of the iPP samples with the hierarchically crystallographic morphologies. It was clear that the crystallization peaks of iPP shifted to higher temperature with NAs. The crystallization temperature of pure iPP, iPP/α-NA, iPP/*β*-NA were 112.8°C, 121.1°C, and 128.2°C, respectively. The NAs exhibited

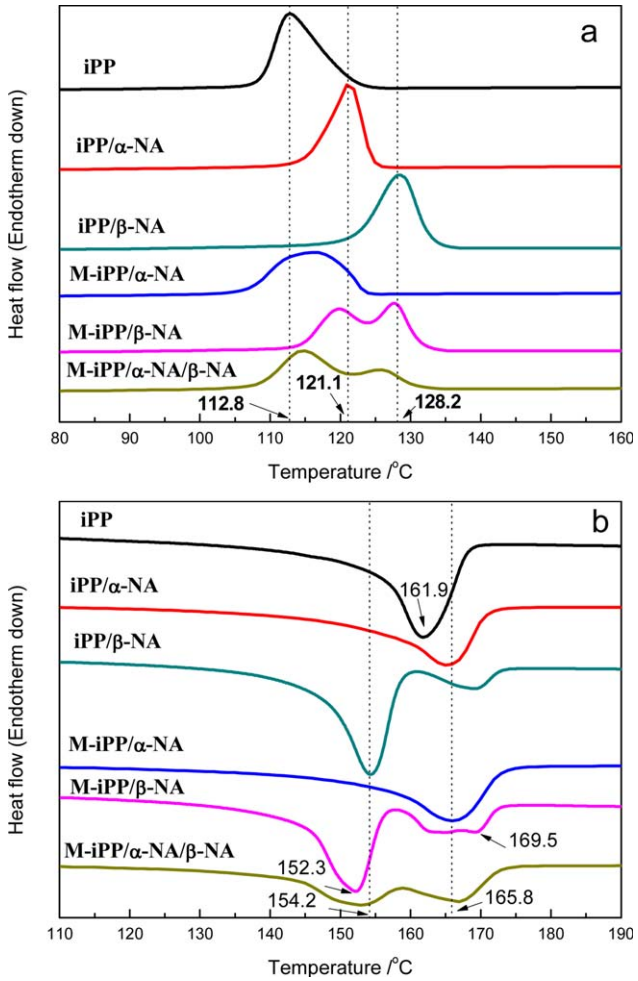

Figure 4. Comparison of DSC cooling (a) and melting (b) curves of the crystal-modified iPP samples with a cooling/heating rate of 10°C/min. [Color figure can be viewed in the online issue, which is available at wileyonlinelibrary.com.]

efficiently to increase the crystallization temperature of iPP. The increased values were 8.3°C and 15.4°C for α-NAs and β-NAs, respectively. These results were ascribed to the stronger heterogeneous nucleation and higher crystal growth rate of β-NAs than that of α-NAs.[46,47] Thus, the β-NAs probably showed the smaller size spherulites and thicker layer of transcrystals than that of α-NAs (Figure 3).

The crystallization behavior of the samples with NAs stratified distribution was much different from the conventional mixing samples. A broad peak ranged from 102.9°C to 124.2°C was found in the M-iPP/α-NA samples resulted from the multiple crystallization behavior which had close crystallization temperature. They included the heterogeneous α-nucleation in the layers decorated with α-NAs, the α-transcrystallization at interfaces and the nucleation (probably another kind heterogeneous α-nucleation[43]) in the pure iPP layers. For the M-iPP/β-NA samples, there were two crystallization peaks at 119.7°C and 127.8°C, which were the temperature of α-nucleation and β-nucleation, respectively. The β-nucleation happened in the layers with β-NAs and the transcrystals, while the α-nucleation existed between the transcrystals in pure iPP layers. There were also two peaks in the M-iPP/α-NA/β-NA samples at 114.7°C and 126.1°C, which were lower than that of corresponding peaks in the M-iPP/β-NA samples. The β-nucleation happened in the layers with β-NAs and the β-transcrystals, while the α-nucleation started in the layers with α-NAs, the α-transcrystals, and the areas between transcrystals in pure iPP layers. The complex crystallization behavior found in the stratified samples is to create the hierarchical crystallographic morphologies.

Figure 4(b) shows the DSC melting curves for the iPP samples with the hierarchically crystallographic morphologies. The peaks around 165°C and 155°C were attributed to the melting of the α-crystals and β-crystals in iPP, respectively.[35] Incorporating α-NAs to iPP leaded to the increased melting temperature of the α-iPP from 161.9°C to 169.5°C. For the samples with α-NAs stratified distribution, the melting temperature peak became much broad, which was ascribed to the different fusion behavior between the α-crystals formed in pure iPP layers and the α-crystals formed in iPP/α-NAs layers.

Interestingly, the iPP/β-NA samples not only mainly exhibited the melting of the β-crystals in iPP at 154.2°C but also some α-crystals at 169.5°C. It was reported that the crystal forms for iPP were determined not only by the type of the nucleating agents but by the crystallization conditions. The α-crystals grow from the surfaces of the β-crystals and vice versa in the several crystallization conditions. These phenomena are called as "re-entrancy".[48,49] These phenomena are caused by the difference between the crystal growth rates for α- and β-crystals. The crystal growth rate for α-crystals is higher than that for the β-crystals in the higher and lower crystallization temperature ranges. However, the rate for β-crystals is higher than that for the α-crystals in the middle crystallization temperature range. As results, the α-crystals selectively grow for the iPP with β-NAs in the higher and lower temperatures and the β-crystals are obtained from the iPP with α-NAs in the middle temperature.

In our case, the samples were prepared by suffering the cooling rate of ca. 40°C/min, and the DSC cooling curves were obtained at the cooling rate of 10°C/min. The DSC melting curves, which used a heating rate of 10°C/min, showed that the iPP with α-NAs showed no β-crystals, while the iPP with β-NAs exhibited some α-crystals. The XRD results also gave the similar results when the samples were prepared at cooling rate of ca. 40°C/min. The results indicated that the "re-entrancy" phenomenon of the α-crystals grow from β-crystals happened in both cooling rates.

For the M-iPP/β-NA samples, the main melting peak still belonged to the β-crystals, which were ascribed to the β-spherulits and β-transcrystals occupying the most space of iPP. However, the proportion of α-crystals in the M-iPP/β-NA samples increased comparing with the iPP/β-NA samples because of the α-nucleation at the centre of the pure iPP layers. The percentage of the α-crystals in the M-iPP/α-NA/β-NA samples further increased due to the α-nucleation at the iPP with α-NAs layers, the centre of the pure iPP layers and the α-transcrystals.

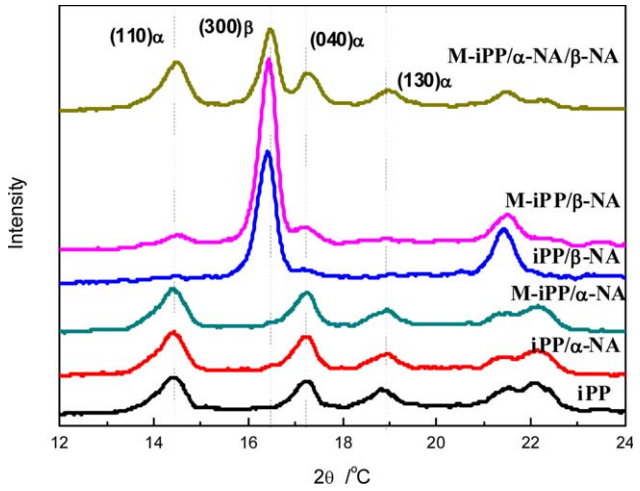

Figure 5. The XRD spectra of the crystal-modified iPP samples. [Color figure can be viewed in the online issue, which is available at wileyonlinelibrary.com.]

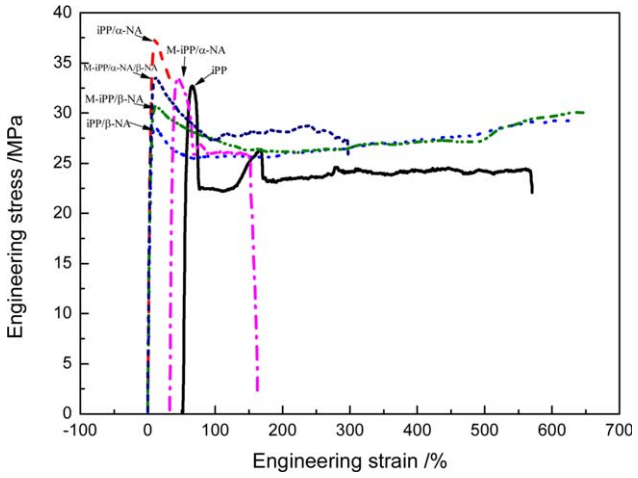

Figure 6. Stress–strain curves of the crystal-modified iPP samples. [Color figure can be viewed in the online issue, which is available at wileyonlinelibrary.com.]

Figure 5 shows the XRD results of the crystallization modified iPP samples. The characteristic peaks at (110), (040), and (130) of α-crystals and no characteristic peaks of β-crystals could be found in pure iPP samples, the iPP/α-NA samples and the M-iPP/α-NA samples. The crystallinity of α-crystals and β-crystals can be calculated from XRD results and summarized in Table I. The crystallinity of iPP slightly increased from 56% to 58% by stratified distribution of α-NAs. The characteristic peak at (300) of β-crystals was found in all the samples with β-NAs. The total crystallinity increased in the iPP samples with nucleating agents stratified distribution. However, the crystallinity of β-crystals decreased from 42% in the iPP/β-NA samples to 38% in the M-iPP/β-NA samples because of the α-crystals in the pure iPP layers. For the M-iPP/α-NA/β-NA samples, the crystallinity of α-crystals reached 38% while the crystallinity of β-crystals decreased to 18% resulting from the increase of α-crystallization behavior.

Mechanical Properties

Figure 6 shows stress-strain curves of the iPP samples with hierarchically crystallographic morphologies which including α-crystals (α-spherulites and α-transcrystals) and β-crystals (β-spherulites and β-transcrystals). The α-spherulites increased stiffness but decreased toughness of iPP, because there were 17% and 15% enhancement on the Young's modulus and yield strength respectively and 94% decreased on the strain at break of iPP incorporated with 0.5 wt % α-NAs. Both of the Young's modulus and the strain at break of the M-iPP/α-NA samples increased comparing with the iPP/α-NA samples resulting from the hierarchically crystallographic morphologies, i.e., two kinds of α-spherulites and the α-transcrystals. It was reported that the α-transcrystals were stiff and brittle in comparison with α-spherulites.[50]

For the iPP/β-NA samples, the Young's modulus and yield strength showed 29% and 13% decrease respectively compared with that of pure iPP. However, their strains at break had 23% higher than that of pure iPP, as shown in Table II. These results indicated that the toughness of iPP with β-spherulites was enhanced because of the β-α polymorphous transition and the loose structure in β-spherulites (compared with α-spherulites).[10] Interestingly, incorporation of the β-transcrytals, the Young's modulus, and yield strength of the M-iPP/β-NA samples were substantially enhanced but without losing the stain at break with the comparison of the iPP/β-NA samples.

Figure 7 gives the comparison study on the fracture surface of the crystal-modified iPP samples after cyro-fracture and tensile fracture at 23°C, respectively. All the samples exhibited the similar cyro-fracture behavior indicating that the hierarchically

Table I. Crystallinity of the Crystal-Modified iPP Samples Calculated from XRD Data (The Equations Can be Found in Ref. 12)

Samples	X_c/%	X_α/%	K_β /%	X_β /%
iPP	56	56	0	0
iPP/α-NA	57	57	0	0
M-iPP/α-NA	58	58	0	0
iPP/β-NA	52	10	80	42
M-iPP/β-NA	54	16	70	38
iPP/α-NA/β-NA	55	38	30	17
M-iPP/α-NA/β-NA	56	38	33	18

Table II. The Young's Modulus, Yield Strength, and Strain at Break of the Crystal-Modified iPP Samples

Samples	Young's modulus/ MPa	Yield strength/ MPa	Strain at break/%
iPP	726 ± 10	32.7 ± 0.2	511 ± 20
iPP/α-NA	851 ± 20	37.5 ± 0.1	33 ± 5
M-iPP/α-NA	956 ± 50	33.6 ± 0.2	131 ± 10
iPP/β-NA	514 ± 50	28.6 ± 0.3	627 ± 50
M-iPP/β-NA	802 ± 50	30.7 ± 0.3	650 ± 50
M-iPP/α-NA/β-NA	820 ± 50	33.6 ± 0.2	298 ± 20
iPP/α-NA/β-NA	742 ± 20	35.6 ± 0.2	25 ± 5

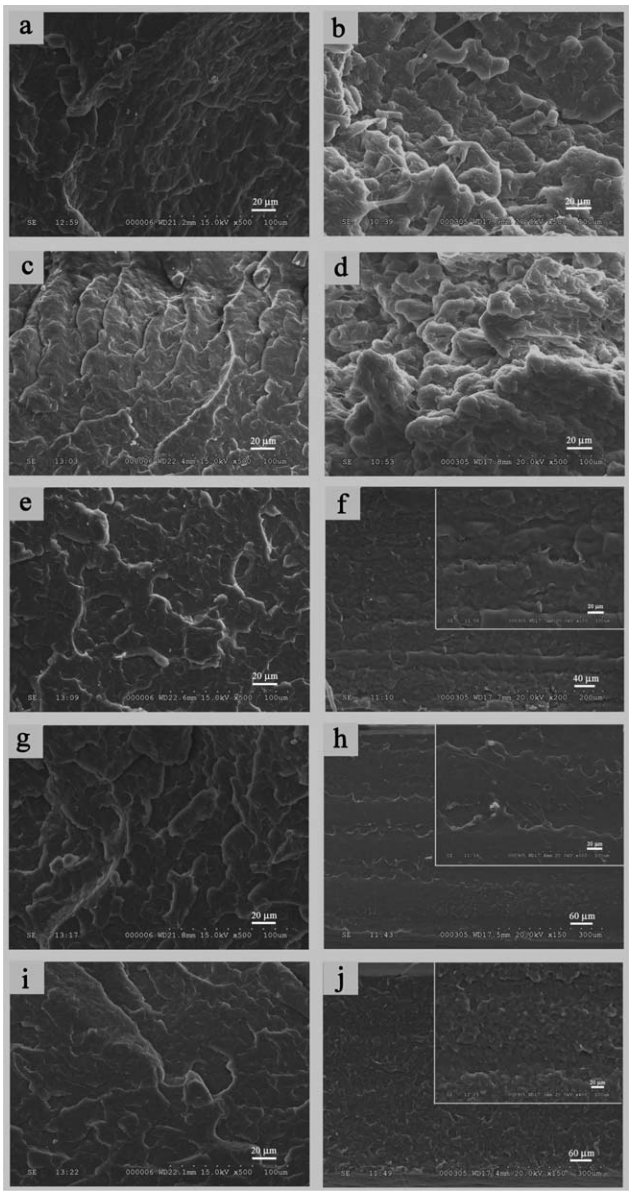

Figure 7. SEM images of the cyro-fracture surface (a, c, e, g, i) and the tensile fracture surface at 23°C (b, d, f, h, j) of the samples: iPP/α-NA (a,b), iPP/β-NA (c, d), M-iPP/α-NA (e, f), M-iPP/β-NA (g, h), M-iPP/α-NA/β-NA (i, j).

crystals all showed brittle at low temperature. However, the tensile fracture surfaces of the samples showed much different from each others. The samples with the stratified distribution of NAs had the layer-by-layer structures, i.e. the pure iPP layers and the layers with NAs. The relatively smooth areas were the pure iPP layers, while the relatively rough areas were the layers with NAs. The pure iPP layers exhibited more brittle than that of the layers with NAs because of the brittle transcrystals formed in the pure iPP layers [Figure 7(f,h,j)]. Comparing with the tensile fracture of the M-iPP/α-NA samples and the M-iPP/β-NA samples, the layers with β-NAs were rougher than that of the layers with α-NAs, which was ascribed to the toughness of β-crystals. These results indicated that the mechanical properties

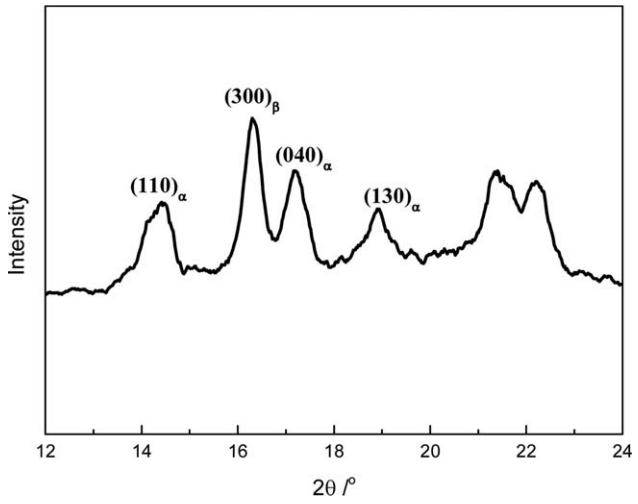

Figure 8. The XRD spectra of the iPP conventional mixed with both α-NAs and β-NAs.

of semicrystalline polymers were mainly dependent on their crystallinity and crystalline morphologies.

For the sake of contrast, the 0.125 wt % α-NAs and 0.125 wt % β-NAs were added into iPP to form α-spherulites and β-spherulites by conventional melt mixing. The samples were named as the iPP/α-NA/β-NA samples. Figure 8 shows the XRD results of the samples. Both of the characteristic peaks of α- and β-crystals were found in the curve indicating that α- and β-spherulites were formed in the iPP/α-NA/β-NA samples. Furthermore, the X_c, X_α, and X_β of the iPP/α-NA/β-NA sample are all close to that of the M-iPP/α-NA/β-NA samples (Table I). Unexpectedly, the iPP/α-NA/β-NA samples did not exhibit both stiffness (α-spherulites) and toughness (β-spherulites). Their Young's modulus and yield strength were slightly higher than that of pure iPP. However, the strain at break declined too much from 511% (pure iPP) to 25%, as shown in Table II. Thus, the addition of both α-NAs and β-NAs into iPP by normal melt

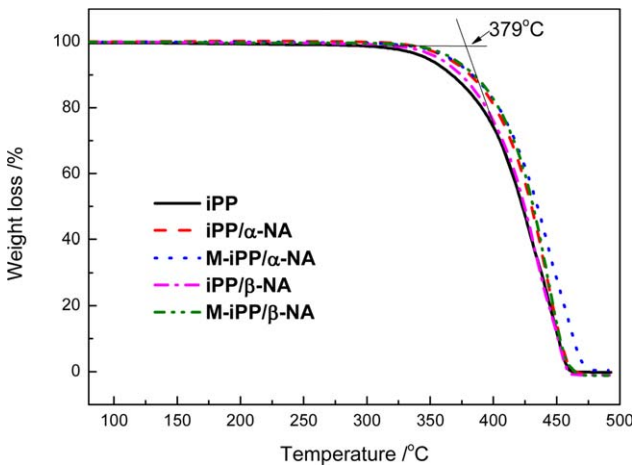

Figure 9. The weight loss curves of iPP with different crystallographic morphologies. [Color figure can be viewed in the online issue, which is available at wileyonlinelibrary.com.]

mixing to form α-spherulites and β-spherulites was not a positive way to improve both stiffness and toughness of iPP.

However, when the α-NAs and β-NAs were stratified distribution in the iPP matrix (the M-iPP/α-NA/β-NA samples), the hierarchically crystallographic morphologies including α-spherulites, α-transcrystals, β-spherulites, and β-transcrystals were created. We found that the Young's modulus and yield strength of the M-iPP/α-NA/β-NA samples increased together with maintaining high strain at break comparing with that of pure iPP and the iPP/α-NA/β-NA samples. The results indicated that the mechanical properties of iPP were not only related to the crystalline modifications but also to the crystalline morphologies, such as spherulites and transcrystals.

Thermal Stability

Figure 9 shows the weight loss curves of the samples with different crystallographic morphologies. All the curves exhibited one-step degradation, which indicated that the addition of α-NAs and β-NAs did not change the decomposition procedure of iPP. The initiate decomposition temperature (T_i) of iPP, iPP/α-NA, M-iPP/α-NA, iPP/β-NA, M-iPP/β-NA samples were 378, 390, 400, 386, and 395°C, respectively. The results illustrated that the thermal stability of iPP could be enhanced by the incorporation of α-NA or β-NA. Furthermore, the samples with stratified distribution of NAs show higher thermal stability than that of normal mixing samples. The results indicated that the transcrystals were probably helpful to improve the thermal stability of iPP. Finally, all the samples were completely degraded which illustrated that the addition of α-NAs and β-NAs did not help the char formation of iPP.

CONCLUSIONS

The hierarchically crystallographic morphologies including α-crystals (α-spherulites and α-transcrystals) and β-crystals (β-spherulites and β-transcrystals) had been successfully fabricated by controlling stratified distribution of the α-NAs and β-NAs. The crystallinity of iPP was slightly enhanced by adding the α-NAs and β-NAs. The β-NAs exhibited stronger heterogeneous nucleation and higher crystal growth rate than that of α-NAs. However, there were still plenty of α-crystals existing in both the iPP/β-NA and M-iPP/β-NA samples because of the "re-entrancy" phenomenon of the α-crystals grow from β-crystals happening in our preparation conditions. The transcrystals showed less ductility than that of the spherulites. The α-spherulites exhibited relatively more stiffness comparing with the β-spherulites. As a result, the iPP with stratified distribution of α-NAs and β-NAs had better mechanical properties and higher thermal stability than that of the iPP directly melt mixing with α-NAs and β-NAs due to the hierarchically crystallographic morphologies.

ACKNOWLEDGMENTS

The authors are grateful to the National Natural Science Foundation of China (51103119), the Natural Science Foundation Project of CQ (CSTC2014JCYJA50024), and the Fundamental Research Funds for the Central Universities (XDJK2014B033) for financial support of this work and the Professor Guo's group in the State Key Laboratory of Polymer Materials Engineering for providing the DSC and POM test in this study.

REFERENCES

1. Padden, F. J.; Keith, H. D. *J. Appl. Phys.* **1959**, *30*, 1479.
2. Turner-Jones, A.; Aizlewood, J. M.; Beckelt, D. R. *Makromol. Chem.* **1964**, *75*, 134.
3. Lotz, B.; Wittmann, J. C.; Lovinger, A. *J. Polymer* **1996**, *37*, 4979.
4. Meille, S. V.; Bruckner, S.; Porzio, W. *Macromolecules* **1990**, *23*, 4114.
5. Mileva, D.; Androsch, R.; Zhuravlev, E.; Schick, C. *Macromolecules* **2009**, *42*, 7275.
6. Ning, N.; Fu, S.; Zhang, W.; Chen, F.; Wang, K.; Deng, H.; Zhang, Q.; Fu, Q. *Prog. Polym. Sci.* **2012**, *37*, 1425.
7. Coulon, G.; Castelein, G.; G'Sell, C. *Polymer* **1999**, *40*, 95.
8. Aboulfaraj, M.; G'Sell, C.; Ulrich, B.; Dahoun, A. *Polymer* **1995**, *36*, 731.
9. Tordjeman, P.; Robert, C.; Marin, G.; Gerard, P. *Eur. Phys. J. E.* **2001**, *4*, 459.
10. Li, X.; Wu, H.; Huang, T.; Shi, Y.; Wang, Y.; Xiang, F.; Zhou, Z. *Colloid Polym. Sci.* **2010**, *288*, 1539.
11. Ferro, D. R.; Meille, S. V.; Brückner, S. *Macromolecules* **1998**, *31*, 6926.
12. Chen, Y. H.; Mao, Y. M.; Li, Z. M.; Hsiao, B. S. *Macromolecules* **2010**, *43*, 6760.
13. Wu, H.; Li, X.; Chen, J.; Shao, L.; Huang, T.; Shi, Y.; Wang, Y. *Compos. Part B* **2013**, *44*, 439.
14. Zhang, B.; Chen, J.; Ji, F.; Zhang, X.; Zheng, G.; Shen, C. *Polymer* **2012**, *53*, 1791.
15. Zhang, B.; Chen, J.; Zhang, X.; Shen, C. *Polymer* **2011**, *52*, 2075.
16. van Erp, T. B.; Balzano, L.; Peters, G. W. M. *ACS Macro Lett.* **2012**, *1*, 618.
17. Wang, Y.; Pan, J.; Mao, Y.; Li, Z.; Li, L.; Hsiao, B. S. *J. Phys. Chem. B* **2010**, *114*, 6806.
18. De Rosa, C.; Auriemma, F. *Angew. Chem. Int. Ed.* **2012**, *51*, 1207.
19. Asakawa, H.; Nishida, K.; Yamamoto, J.; Inoue, R.; Kanaya, T. *Polymer* **2012**, *53*, 2777.
20. Sadeghi, F.; Ajji, A.; Carreau, P. *J. Polym. Eng. Sci.* **2007**, *47*, 1170.
21. Tabatabaei, S. H.; Carreau, P. J.; Ajji, A. *Polymer* **2009**, *50*, 4228.
22. Huan, Q.; Zhu, S.; Ma, Y.; Zhang, J.; Zhang, S.; Feng, X.; Han, K.; Yu, M. *Polymer* **2013**, *54*, 1177.
23. Ma, Z.; Fernandez-Ballester, L.; Cavallo, D.; Gough, T.; Peters, G. W. M. *Macromolecules* **2013**, *46*, 2671.
24. Wang, K.; Chen, F.; Li, Z. M.; Fu, Q. *Prog. Polym. Sci.* **2014**, *39*, 891.
25. Zhang, Y.; Zhang, J.; Qian, X.; Deng, P.; Shen, K. *Polymer* **2012**, *53*, 4318.

26. Li, Y.; Liao, Y.; Gao, X.; Yuan, Y.; Ke, W.; Shen, K. *J. Polym. Sci. Part B: Polym. Phys.* **2005**, *43*, 13.
27. Zhong, G.; Li, L.; Mendes, E.; Byelov, D.; Fu, Q.; Li, Z. *Macromolecules* **2006**, *39*, 6771.
28. Lin, Y.; Hiltner, A.; Baer, E. *Polymer* **2010**, *51*, 5807.
29. Xu, S.; Wen, M.; Li, J.; Guo, S.; Wang, M.; Du, Q.; Shen, J.; Zhang, Y.; Jiang, S. *Polymer* **2008**, *49*, 4861.
30. Quan, H.; Zhong, G.; Li, Z.; Yang, Y.; Xie, B.; Yang, S. *Polym. Eng. Sci.* **2005**, *45*, 1303.
31. Li, Z.; Li, L.; Shen, K.; Yang, W.; Huang, R.; Yang, M. *Macromol. Rapid Commun.* **2004**, *25*, 553.
32. Chen, Y. H.; Huang, Z. Y.; Li, Z. M.; Tang, J. H.; Hsiao, B. S. *RSC Adv.* **2014**, *4*, 14766.
33. Zhang, Y.; Zhang, L.; Liu, H.; Du, H.; Zhang, J.; Wang, T.; Zhang, X. *Polymer* **2013**, *54*, 6026.
34. Luo, F.; Geng, C.; Wang, K.; Deng, H.; Chen, F.; Fu, Q.; Na, B. *Macromolecules* **2009**, *42*, 9325.
35. Liu, M.; Guo, B.; Du, M.; Chen, F.; Jia, D. *Polymer* **2009**, *50*, 3022.
36. Chen, Y. H.; Zhong, G. J.; Wang, Y.; Li, Z. M.; Li, L. B. *Macromolecules* **2009**, *42*, 4343.
37. Li, H.; Yan, S. *Macromolecules* **2011**, *44*, 417.
38. Wang, C.; Liu, C.-R. *Polymer* **1999**, *40*, 289.
39. Wang, C.; Liu, F.; Huang, W. *Polymer* **2011**, *52*, 1326.
40. Pompe, G.; Mader, E. *Compos. Sci. Technol.* **2000**, *60*, 2159.
41. Quan, Y.; Li, H.; Yan, S. *Ind. Eng. Chem. Res.* **2013**, *52*, 4772.
42. Assouline, E.; Pohl, S.; Fulchiron, R.; Gérard, J.-F.; Lustiger, A.; Wagner, H. D.; Marom, G. *Polymer* **2000**, *41*, 7843.
43. Wang, M.; Lin, L.; Peng, Q.; Ou, W.; Li, H. *J. Appl. Polym. Sci.* **2014**, *131*, 39632.
44. Qiu, F.; Wang, M.; Hao, Y.; Guo, S. *Compos. A* **2014**, *58*, 7.
45. Somani, R. H.; Hsiao, B. S.; Nogales, A.; Fruitwala, H.; Srinivas, S.; Tsou, A. H. *Macromolecules* **2001**, *34*, 5902.
46. Lovinger, A. J.; Chua, J. O.; Gryte, C. C. *J. Polym. Sci. Polym. Phys. Ed.* **1977**, *15*, 641.
47. Keith, H. D.; Padden, F. J., Jr.; Walter, N. M.; Wickoff, H. W. *J. Appl. Phys.* **1959**, *30*, 1485.
48. Lotz, B. *J. Macro. Sci. B* **2002**, *41*, 685.
49. Varga, J. *J. Macro. Sci. B* **2002**, *41*, 1121.
50. Folkes, M. J.; Hardwick, S. T. *J. Mater. Sci. Lett.* **1987**, *6*, 656.